Al-Azhar Bulletin of Science

Volume 34 | Issue 1 Article 1

2023
Section: Earth science

# Geoelectric Evaluation of Soil Foundation Utilizing Electrical Resistivity Tomography at West Gulf of Suez, Al-Ain Al Sokhna, Egypt

Mahmoud Zayed
*Geology Department, Faculty of Science, Al-Azhar University, Cairo 11884, Egypt*, m_zayed@azhar.edu.eg



## How to Cite This Article

Zayed, Mahmoud (2023) "Geoelectric Evaluation of Soil Foundation Utilizing Electrical Resistivity Tomography at West Gulf of Suez, Al-Ain Al Sokhna, Egypt," *Al-Azhar Bulletin of Science*: Vol. 34: Iss. 1, Article 1.
DOI: https://doi.org/10.58675/2636-3305.1635

# Geoelectric Evaluation of Soil Foundation Utilizing Electrical Resistivity Tomography at West Gulf of Suez, Al-Ain Al Sokhna, Egypt

## Cover Page Footnote

Acknowledgments The author would like to thank the management of CAVO Resort Ain Sokhna for the hospitality during the fieldwork and to thank the editor and anonymous reviewers for their constructive comments and suggestions, which significantly improved the quality of this research Statements and Declarations Funding: No funding was received for conducting this study. Conflicts of interest Declaration of interest statement: The author reports there are no competing interests to declare.

ORIGINAL ARTICLE

# Geoelectric Evaluation of Soil Foundation Utilizing Electrical Resistivity Tomography at West Gulf of Suez, Al-Ain Al Sokhna, Egypt

Mahmoud Zayed*

Geology Department, Faculty of Science, Al-Azhar University, Cairo, Egypt

**Abstract**

**To evaluate the subsurface layers and geological structures for construction in one of the tourist areas in Egypt, the geoelectrical survey was used, represented by the two-dimensional Electrical Resistivity Tomography (ERT). The geoelectrical survey includes 16 ERT profiles that have been conducted by using the Winner electrode array with twenty electrodes connected to a multi-core cable. The electrode spacing (a) varies between 4 and 6 m to investigate a depth of around twenty meters, and the length of the ERT profiles varies from 76 to 114 m depending on the electrode spacing difference and the field's available space. Through the geoelectric results that are confirmed by drilling of six boreholes, five geoelectric layers were identified, in addition to six faults inferred from the geoelectrical results. These faults are concentrated in the north of the research area. Shale and shaly-sand layers were among the examined geoelectric layers that were found on a small scale in the research region. Because of the major impact that these layers have on buildings, it was advised that the required engineering solutions be developed for these layers.**

*Keywords:* Al-Ain Al Sokhna, Electrical resistivity tomography, Soil foundation, Wenner array, West Gulf of Suez

## 1. Introduction

The research area is directly adjacent to the Suez-Hurghada Road and is situated west of the Gulf of Suez in Al-Ain Al Sokhna, Egypt (Fig. 1). It is an important area from a touristic point of view, as it contains many existing tourist resorts, and there are plans for expansion in the construction and reconstruction. Near the study area, to the west, there is the Galala plateau, where a giant project is being built to build an integrated new city called Galala City. Therefore, it is crucial to conduct a geophysical study to assess the soil for construction, which is the main objective of this research. So, a geoelectric survey was conducted on a part of the resort's area, Al-Ain Al Sokhna, to detect the lithology and the lateral/vertical changes of the subsurface layers. In addition, to determine the structure (faults) affecting the investigated area up to twenty meters depth. To achieve the aims, the Electrical Resistivity Tomography (ERT) by using the Wenner array was utilized. In addition to that six boreholes were drilled to confirm the geoelectric results. The two-dimensional ERT is commonly used to map geologically complex terrain Griffiths and Barker [1]. Typically, 20 electrodes attached to an automated multi-core cable are used to conduct these surveys. In recent years, the introduction of automated data acquisition and inversion has expanded the practical applicability of resistivity imaging. The technique is currently frequently employed in the fields of engineering and environmental science Dahlin [2].

## 2. General geologic setting

Geologically, the exposed surface rock units in the research area and their surroundings range in age from Upper Cretaceous to Holocene (Fig. 2) Klitzsch

Received 25 October 2022; revised 5 December 2022; accepted 16 December 2022.
Available online 23 August 2023

* Geology Department, Faculty of Science, Al-Azhar University, Cairo, 11884, Egypt. Fax: (0020/2) 22629356.
E-mail address: m_zayed@azhar.edu.eg.

https://doi.org/10.58675/2636-3305.1635

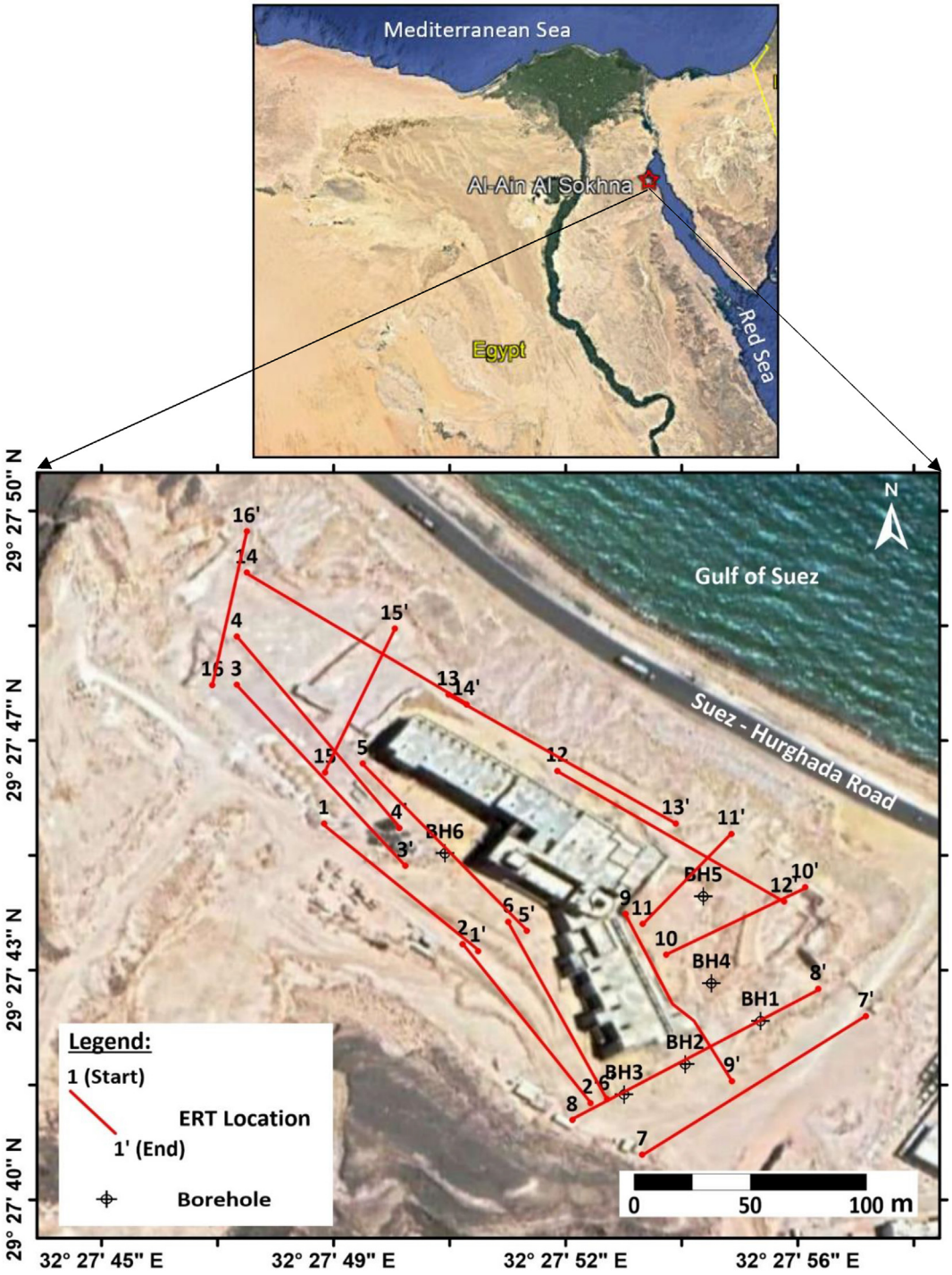


*Fig. 1. Google earth image showing the ERT profiles location and the available drilled boreholes.*

and colleagues [3]. These units are as follows: Firstly, the oldest exposed surface rock unit of the study area is represented by Aheimer Formation (Upper Carboniferous-Lower Permian). The Aheimer Formation is composed of dark-colored sandstone (cross-bedded sandstone and an alternating thick bed of sandstone), shale, and clay. It reaches a thickness of 250 m at the type locality of Wadi Aheimer, which is located within the Galala plateau's eastern cliff Abdallah and El Adin [4] and extends to the Al-Ain Al Sokhna area. The Permo-Triassic reddish-brown clastic sediments are exposed along

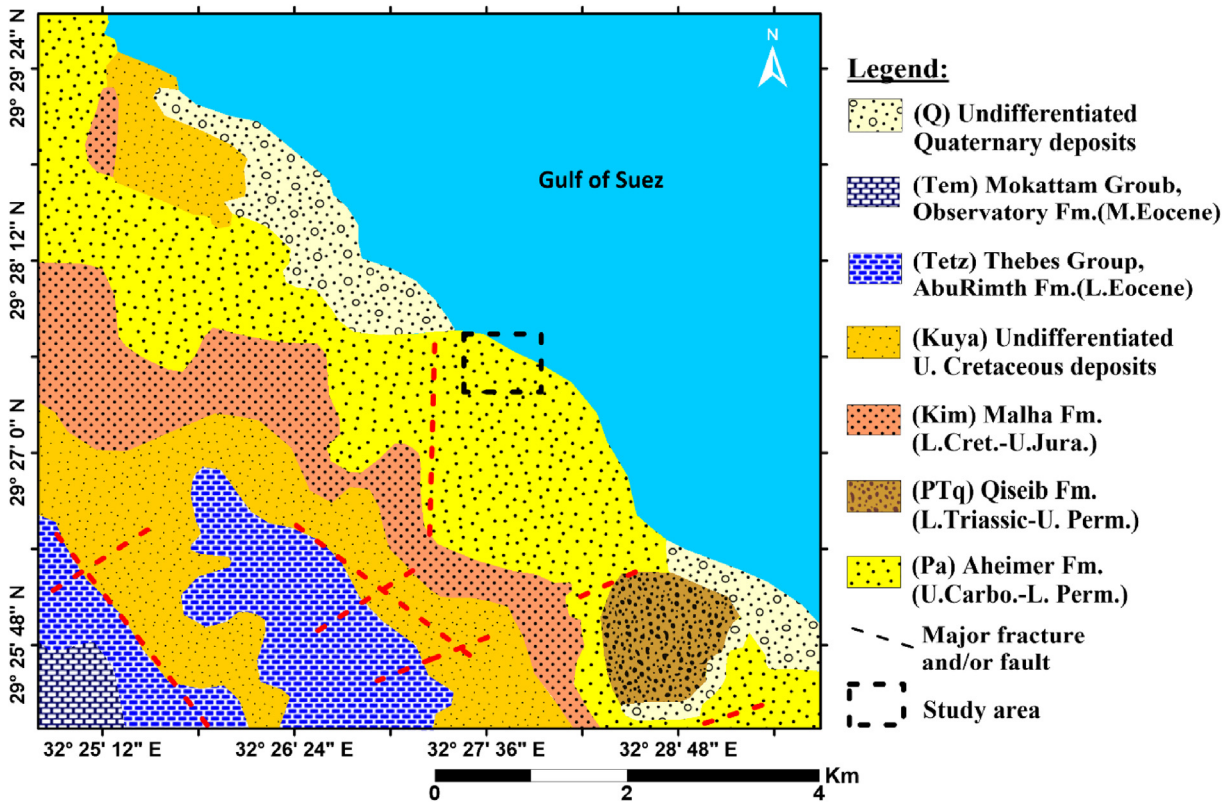


*Fig. 2. Geologic map of the west Gulf of Suez Area, Egypt, showing the study area by a dotted square (after [3]).*

Wadi Qiseib around the Port Sokhna Resort as a Qiseib Formation Abdallah and colleagues [5]. It rests conformably above the Aheimer Formation, and it is unconformably overlain by the Malha Formation of the Lower Cretaceous - Upper Jurassic sandstone, while the Upper Cretaceous rocks are represented by undifferentiated deposits Abdelazeem and colleagues [6]. Secondly, the Tertiary rocks are represented by the Thebes Group (Abu Rimth Formation of well-bedded shelf limestone) of Lower Eocene, and the Mokattam Group (Consisting of Observatory Formation of shallow marine limestone with Giushi Formation) of Middle Eocene. Finally, the Quaternary deposits are represented by undifferentiated deposits of alluvial fans, wadi deposits, sand, gravel, and coastal deposits Klitzsch and colleagues [3].

Structurally, Normal faults with sinuous trends that strike generally parallel to the rift and delimit multiple tilted blocks dominate the structure of the Gulf of Suez rift Said [7], while there is limited evidence for left-lateral strike-slip motion along N–S trending faults Garfunkle and Bartov [8] and Chenet and colleagues [9]. Furthermore, the interpretation of Landsat imagery reveals that the more recent normal faults strike primarily N–S along the Gulf's eastern side Tapponnier and Armijo [10]. The rock units of the research area belong to the Paleozoic age which means that these rocks were affected by the tectonic evolution of the Suez Gulf. Consequently, it caused the appearance of several sets of faults. Many authors reported that the faults existing on the western side of the Gulf of Suez have three main direction sets including NW–SE, E–W, and NNW-SSE, and the dominant fault trend takes the Gulf of Suez direction Said, Abdallah, Arnous and colleagues [7,11–13].

## 3. Materials and methods

### *3.1. Test method and measurement procedure*

The two-dimensional ERT is used to map areas with moderately complex geology Griffitths and Barker [1]. Several researchers, including Cardarelli and colleagues, Dhamiry and Zouaghi [14–26], have employed the ERT for foundation evaluation reasons. The survey in this research was conducted using a Wenner array with twenty electrodes connected to a multi-core cable to detect the lithology and the structure (faults) affecting the investigated area. The most common setup for a two-dimensional survey of the Wenner array with twenty electrodes alongside a direct line connected to a

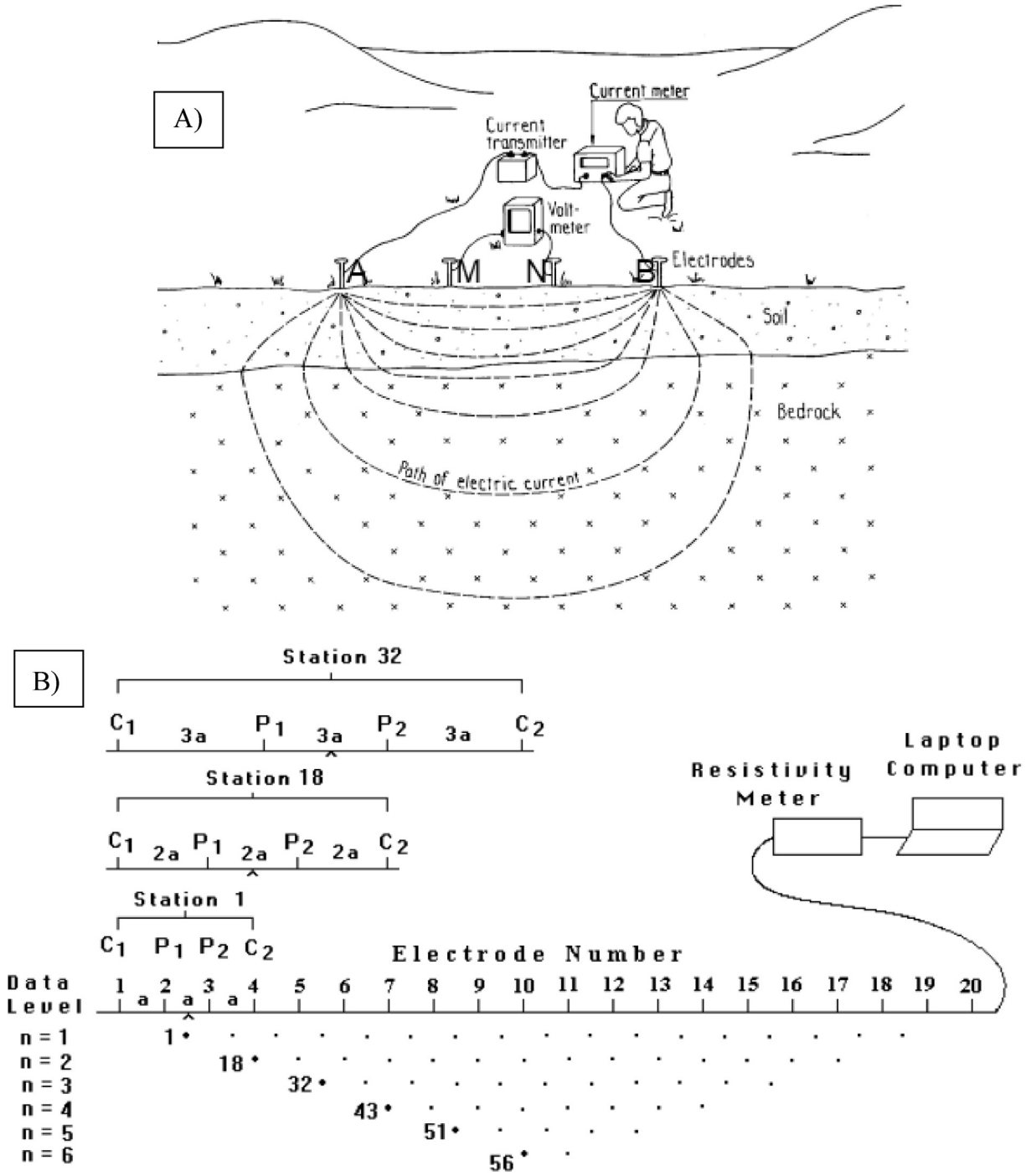


*Fig. 3. (a) Sketch showing the principle of DC resistivity measurement (after [2]), (b) The arrangement of electrodes for a 2-D electrical Wenner survey and the sequence of measurements used to build up a pseudo-section (after [27]).*

multi-center cable (Fig. 3). Usually, a consistent spacing (a) among adjoining electrodes is used. The multi-center cable is connected to a digital switching unit linked to a PC. The sequence of measurements to take, the type of array to employ, and other survey characteristics (such as current, spacing, and stacking) are often input into a text file that can be read by laptop software. After reading the control file, the computer program then automatically selects the appropriate electrodes for each measurement. The spacing between neighboring electrodes in the Wenner array, as shown in Fig. 3, is 'a.' The initial stage is to use the Wenner array with an electrode spacing of '1a' to take all measurements.

Electrodes 1, 2, 3, and 4 are used for the first measurement. Notice how electrode (1) serves as the first current electrode C1, electrode (2) serves as the first potential electrode P1, electrode (3) serves as the second potential electrode P2, and electrode 4 serves as the second current electrode C2. Electrodes 2, 3, 4, and 5 are used for C1, P1, P2, and C2 measurements, respectively. After that, the measurements are taken automatically and stored in the computer Loke [27].

### 3.2. Field survey method

Topographic and geoelectric surveys are as follows: The topographic survey was conducted to determine the location (latitude and longitude) of the ERT profile on the topographic map by using the GPS apparatus (Trimble type contact with twelve satellites) and concluding the ground elevation (Table 1). The geoelectrical survey was performed using GD-10 Supreme instrument (Fig. 4) based on the multi-functional direct current (DC) method. Regular ERT survey setups and subsurface profiling utilizing two-dimensional survey arrays is supported [28]. The geoelectrical survey includes sixteen ERT profiles (from ERT 1 to ERT 16), that have been carried out in the research area by using the Winner electrode array. The ERT profiles were chosen to be perpendicular to each other to give a clear picture of subsurface lithology and detect possible structure features in all directions, as shown in the ERT profile's location map Fig. 1. The Wenner electrode array adopted twenty steel electrodes to conduct the electric current and voltage measurements along with the profiles. Also, shows the electrode switching sequence and the corresponding subsurface coverage that allows the two-dimensional resistivity imaging. The electrode spacing (a) has been chosen according to the available surface length which ranges between 4 and 6 m (Table 1). The extension of the ERT profiles varies from 76 to 114 m based on the difference in electrode spacing considering the available distance at the field (Fig. 4). Six boreholes of twenty meters in depth were drilled to integrate the results of the boreholes and the geoelectric (Fig. 5).

### 3.3. Data processing

After the field survey, the apparent resistivity was converted into an interpretable resistivity model section. The collected apparent-resistivity raw data was dumped from the resistivity meter using Geomative software 'Geomative Studio V2. 4P1_0225_T35'. The data file was then introduced to processing two-dimensional-resistivity tomography software 'RES2DINV'. The first step in processing the apparent resistivity data is to manage bad data points. Such bad data points should be removed before a final interpretation is made. Using the commercial software (RES2DINV), the true-resistivity values are inverted from apparent resistivity values. The inversion process is based on a quasi-Newton optimization technique that implements smoothness-limited least-squares inversion.

## 4. Results and discussion

The produced inverse model resistivity sections of all profiles indicate the presence of five geo-

*Table 1. Geographic location and geoelectric survey parameters of the ERT profiles.*

| ERT No. | The first electrode location (Start point) | | | The end electrode location (End point) | | | Spacing 'a' (m) | ERT Length (m) | Exploration depth (m) | ERT Direction |
|---|---|---|---|---|---|---|---|---|---|---|
| | Latitude (N) | Longitude (E) | Attitude | Latitude (N) | Longitude (E) | Attitude | | | | |
| ERT1 | 29°27′45.50″ | 32°27′48.45″ | 52 | 29°27′43.38″ | 32°27′50.95″ | 41 | 5 | 95 | 17 | NW–SE |
| ERT2 | 29°27′43.61″ | 32°27′50.60″ | 42 | 29°27′41.12‘ | 32°27′52.58″ | 34 | 5 | 95 | 17 | NW–SE |
| ERT3 | 29°27′47.67″ | 32°27′47.09″ | 58 | 29°27′44.83″ | 32°27′49.71″ | 47 | 6 | 114 | 21 | NW–SE |
| ERT4 | 29°27′48.43″ | 32°27′47.10″ | 52 | 29°27′45.20″ | 32°27′49.87″ | 48 | 6 | 114 | 21 | NW–SE |
| ERT5 | 29°27′46.44″ | 32°27′49.05″ | 47 | 29°27′43.82″ | 32°27′51.60″ | 38 | 5 | 95 | 17 | NW–SE |
| ERT6 | 29°27′43.96″ | 32°27′51.31″ | 40 | 29°27′41.18″ | 32°27′52.84″ | 33 | 5 | 95 | 17 | NW–SE |
| ERT7 | 29°27′40.31‘ | 32°27′53.39‘ | 32 | 29°27′42.48‘ | 32°27′56.86‘ | 19 | 6 | 114 | 21 | NE–SW |
| ERT8 | 29°27′40.85″ | 32°27′52.30″ | 35 | 29°27′42.80″ | 32°27′55.94″ | 21 | 6 | 114 | 21 | NE–SW |
| ERT9 | 29°27′44.08″ | 32°27′53.13″ | 31 | 29°27′40.95″ | 32°27′55.10″ | 27 | 6 | 114 | 21 | NNW-SSE |
| ERT10 | 29°27′43.44″ | 32°27′53.76″ | 29 | 29°27′44.50″ | 32°27′55.91″ | 20 | 4 | 76 | 14 | NE–SW |
| ERT11 | 29°27′43.92″ | 32°27′53.39″ | 31 | 29°27′45.34″ | 32°27′54.77″ | 24 | 4 | 76 | 14 | NE–SW |
| ERT12 | 29°27′46.30″ | 32°27′52.02″ | 31 | 29°27′44.28″ | 32°27′55.59″ | 21 | 6 | 114 | 21 | NW–SE |
| ERT13 | 29°27′47.52″ | 32°27′50.38″ | 38 | 29°27′45.50″ | 32°27′53.91″ | 27 | 6 | 114 | 21 | NW–SE |
| ERT14 | 29°27′49.43″ | 32°27′47.25″ | 42 | 29°27′47.37″ | 32°27′50.66″ | 36 | 6 | 114 | 21 | NW–SE |
| ERT15 | 29°27′46.30″ | 32°27′48.47″ | 50 | 29°27′48.55″ | 32°27′49.55″ | 37 | 4 | 76 | 14 | NE–SW |
| ERT16 | 29°27′47.67″ | 32°27′46.72″ | 59 | 29°27′50.08″ | 32°27′47.25″ | 36 | 4 | 76 | 14 | NNE-SSW |


*Fig. 4. The geomative GD-10 supreme instrument, field photos for the equipment, and setup of the ERT survey.*

electrical layers and some geoelectric inferential faults (Fig. 6). These geoelectric results are deduced from variations in resistivity in both vertical and horizontal directions.

### *4.1. Geoelectric layers*

The first Geoelectrical layer (Surface layer): This layer represents the upper surface layer; it has resistivity values between 10 and 90 Ohm. m. The thickness of this layer varies from 5 to 13 m and is composed of dumping or backfilling materials from dry sand, shale, gravel, and rock fragments.

The second geoelectrical layer (Sandstone): This layer observed at all the ERT profiles represents the second subsurface layer. The resistivity values of this layer range from 30 to 300 Ohm.m, and its thickness ranges from 5 to 15 m. It is mainly composed of sandstone.

The third geoelectrical layer (Massive Sandstone): This layer has a wide distribution in the investigated area, where observed at most ERT profiles. It has a wide range of resistivity that ranges from 300 to 5000 Ohm.m. The thickness of this layer ranges between 8 and 16 m. The end of this layer was not detected in some other profiles within the range of exploration depth. It is composed of massive sandstone.

The fourth geoelectrical layer (Shaly sandstone): This layer is observed only at ERT profiles numbers 8 and 12 (Fig. 6). It has relatively low resistivity values ranging from 10 to 30 Ohm.m, the end of this

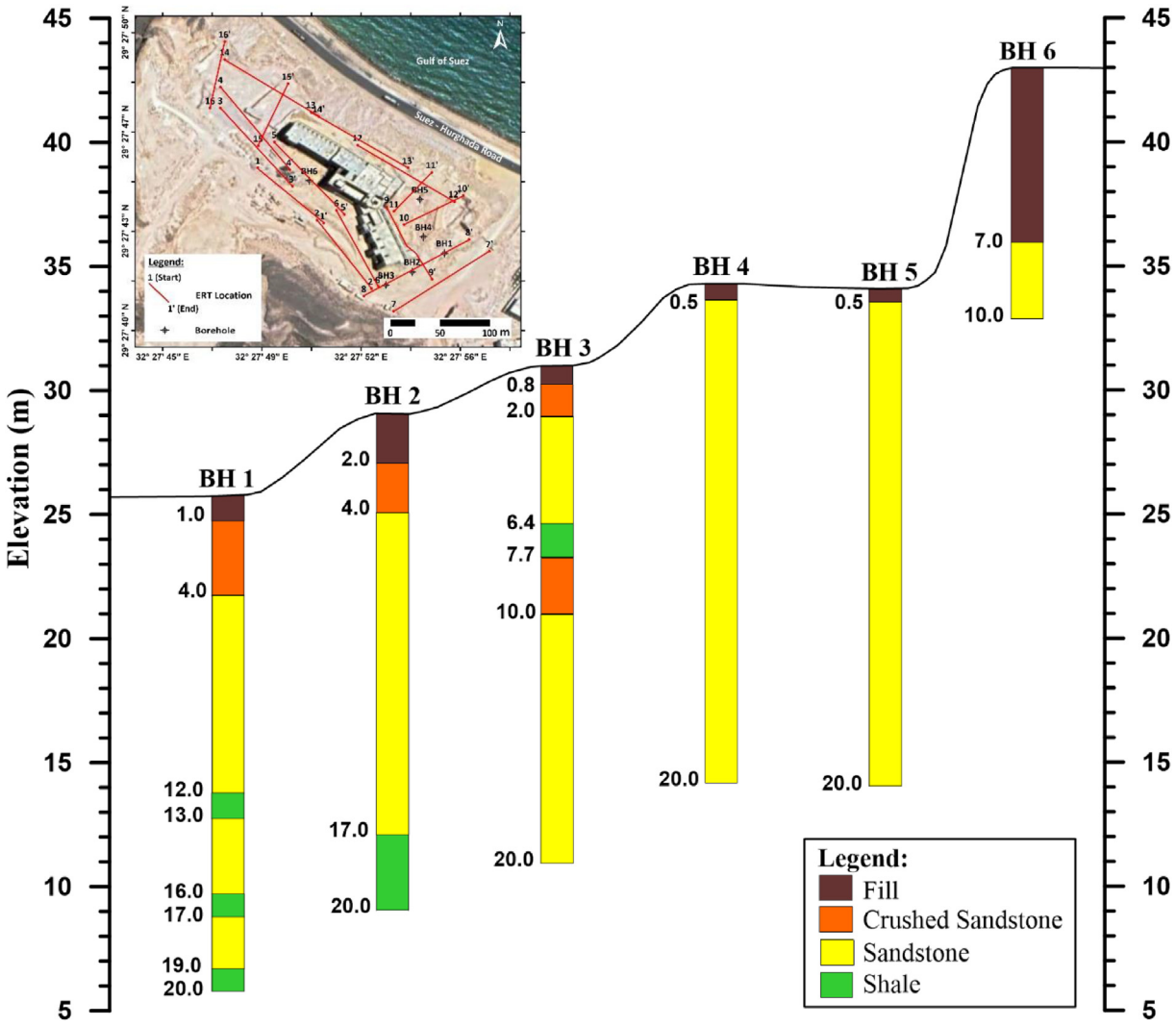


*Fig. 5. The lithology of the available boreholes.*

layer is not observed because it is located at the end of the mentioned ERT profiles. It is composed of shaly sandstone or sandstone with a high amount of shale intercalation.

The fifth geoelectrical layer (Shale): This layer is observed only in the eastern part of the investigated area, at the ERT profiles No. 9 and 10 (Fig. 6). It has extremely low resistivity values ranging from 1 to 10 Ohm.m. This layer is observed at a depth ranging from 9 to 14 m from the ground surface, and the end of this layer is not observed because it exists at the end of the two mentioned ERT profiles. It is composed of shale.

### *4.2. Geoelectric inferential structure*

The ERT profiles indicate the presence of six geoelectrical inferential faults (from F1 to F6) distributed over the investigated area (Fig. 6). The first inferential fault F1 is observed at ERT profile No. 12 and the second one F2 at ERT profile No. 14. The rest of the faults are distributed over two ERT profiles, where every two faults were observed in one ERT. They are distributed as follows: F3 and F4 were observed at ERT 15, in addition, F5 and F6 were observed at ERT 16. These faults may connect considering the geoelectrical results and field observations to give two connected faults in the north part of the investigated area (Fig. 7).

## 5. Summary and conclusion

This study focuses on the subsurface layer and structure affecting the investigation area by using an ERT survey. Considering ERT profile results, which

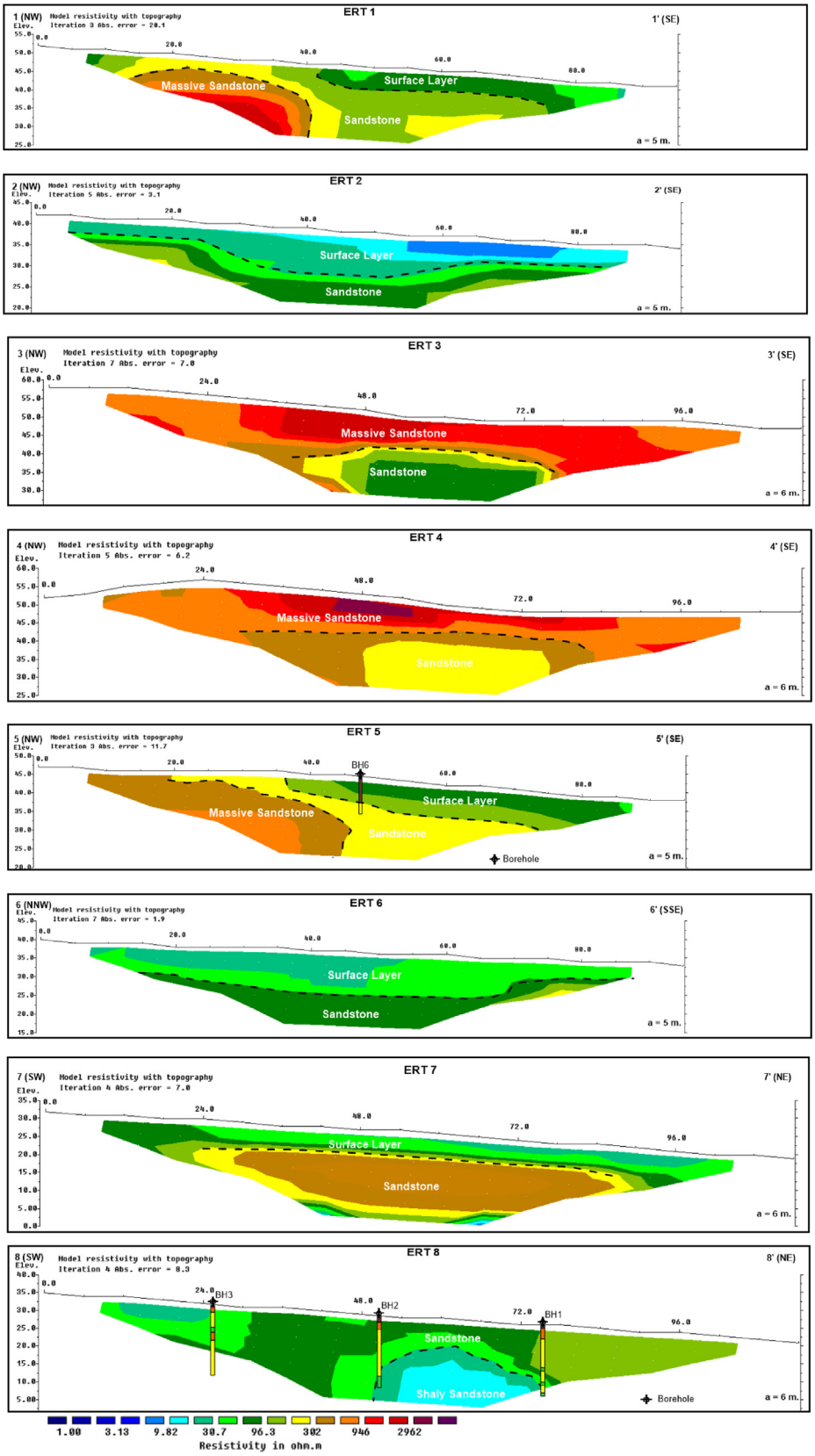


*Fig. 6 The inverse resistivity cross-section for ERT profiles.*

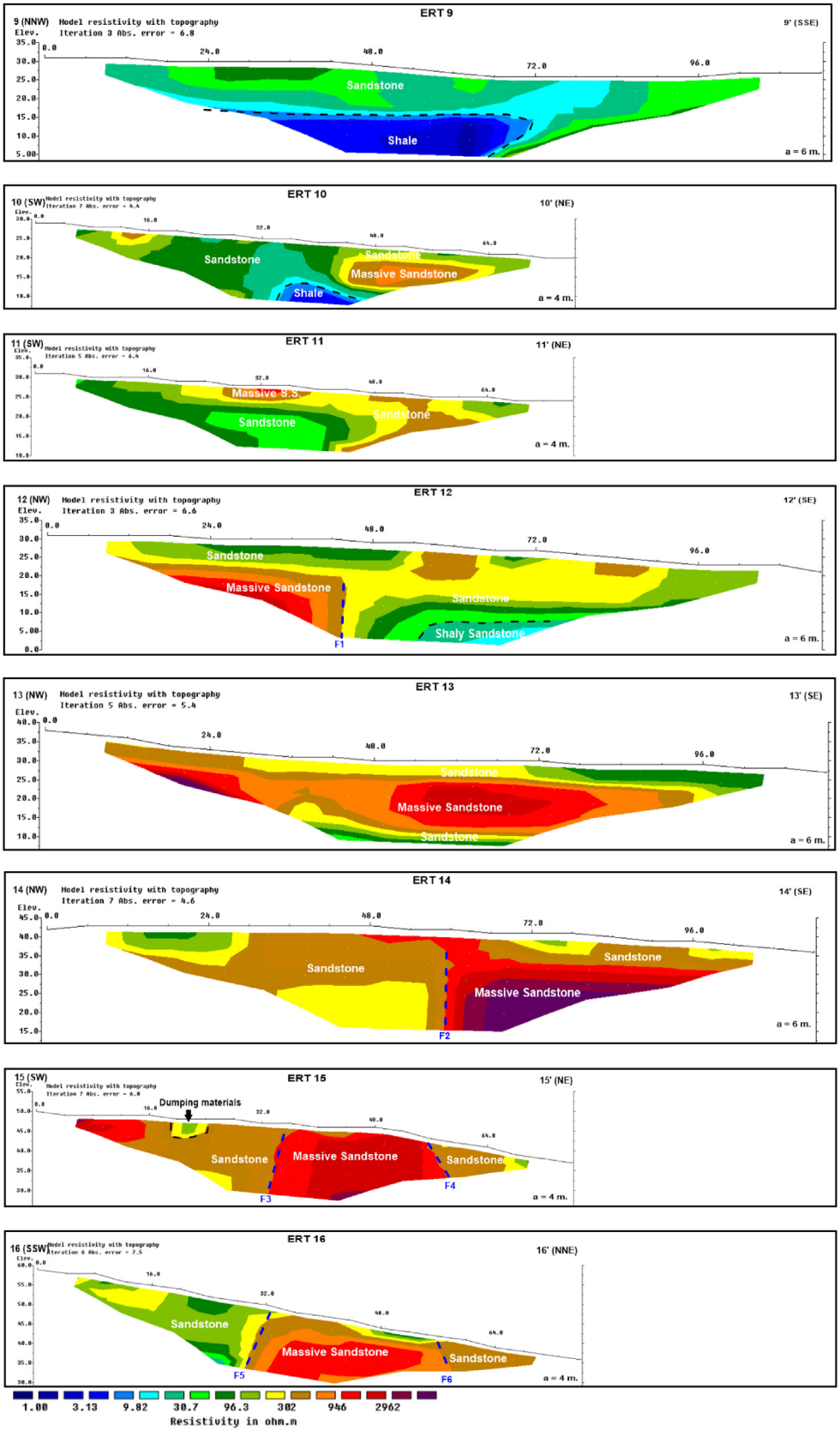


*Fig. 6 (Continued).*

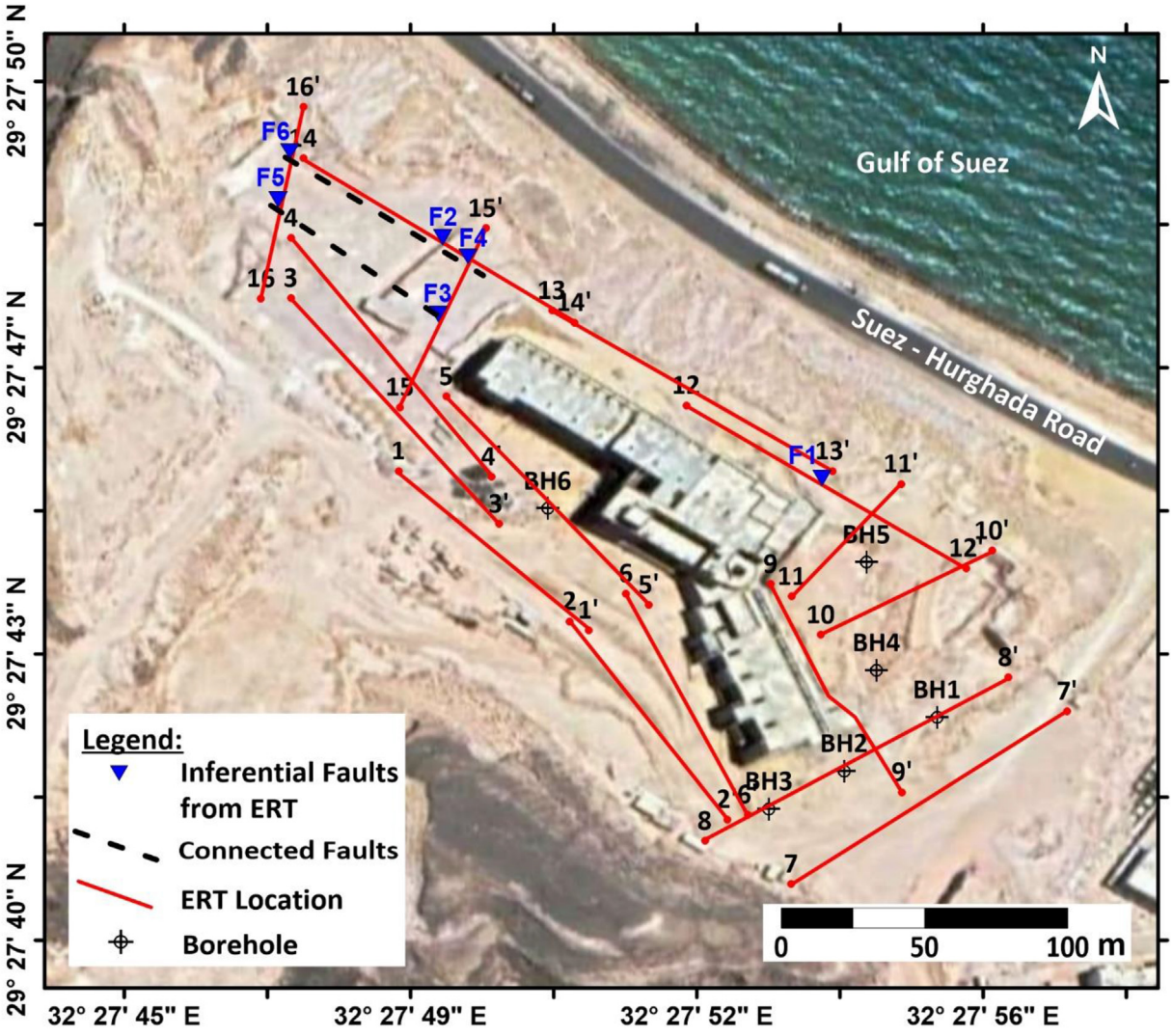


*Fig. 7. The distribution of geoelectrical inferential faults (from F1 to F6) over the investigated area and suggested connected faults.*

can be concluded there are five geo-electrical layers and some geoelectric inferential faults.

### 5.1. Geoelectric layers

The first Geoelectrical layer (Surface layer) represents the upper surface layer; it has resistivity values that vary from 10 to 90 Ohm.m, and its thickness ranges from 5 to 13 m. It is composed of dumping or backfilling materials from dry sand, shale, gravel, and rock fragments. The second geoelectrical layer (Sandstone) was observed in all the ERT profiles. The resistivity values of this layer range from 30 to 300 Ohm.m and its thickness range from 5 to 15 m. It is composed of sandstone. The third geoelectrical layer (Massive Sandstone) has a wide distribution in the study area, where observed in most ERT profiles. It has a wide range of resistivity that ranges from 300 to 5000 Ohm.m. Its thickness ranges from 8 to 16 m, while the end of this layer is undetectable in some other profiles, within the range of exploration depth. It is composed of massive sandstone. The fourth geoelectrical layer (Shaly sandstone) is observed only in the eastern part of the research area, at profiles No. 8 and 12. It has low resistivity values ranging from 10 to 30 Ohm.m, the end of this layer is not observed because it is located at the end of the mentioned ERT profiles. It is composed of shaly sandstone or sandstone with a high amount of shale intercalation. The fifth geoelectrical layer (Shale) is observed only in the ERT profiles No. 9 and 11. It has incredibly low resistivity values ranging from 1 to 10 Ohm.m. This layer is observed at depth ranges from 9 to 14 m from the ground surface and the end of this layer is not observed because it is located at the end

of the mentioned ERT profiles. It is composed of shale.

### 5.2. Geoelectric inferential structure

The ERT profiles indicated that there are six geo-electrical inferential faults (from F1 to F6) distributed over the investigated area. The first inferential fault F1 is observed at ERT profile No. 12 and the second fault F2 at ERT profile No. 14. As for the rest of the six inferential faults, they are distributed over three ERT profiles, where every two faults were observed in one ERT, and they are distributed as follows: F3 and F4 are observed at ERT No. 15, F5 and F6 are observed at ERT No. 16. These faults may connect considering the geo-electrical results and field observations to give two connected faults in the north part of the investigated area.

### 5.3. Recommendations

(1) The shale layer observed at ERT profiles No.9 and 1 (Figs. 6 and 8) at the eastern part of the hotel's building could affect the stability of the construction. Hence, it is recommended to conduct an engineering study to find out the effect of this layer on the existing building and find structural solutions that prevent or decrease the effect of this layer.
(2) In addition, it is recommended to study the impact of the observed faults (Fig. 8) in the eastern part of the research area on the existing hotel building and how to deal with it from an engineering point of view.
(3) It is counseled to avoid the area located north-west of the investigated area in the event of new construction work, as it is affected by the

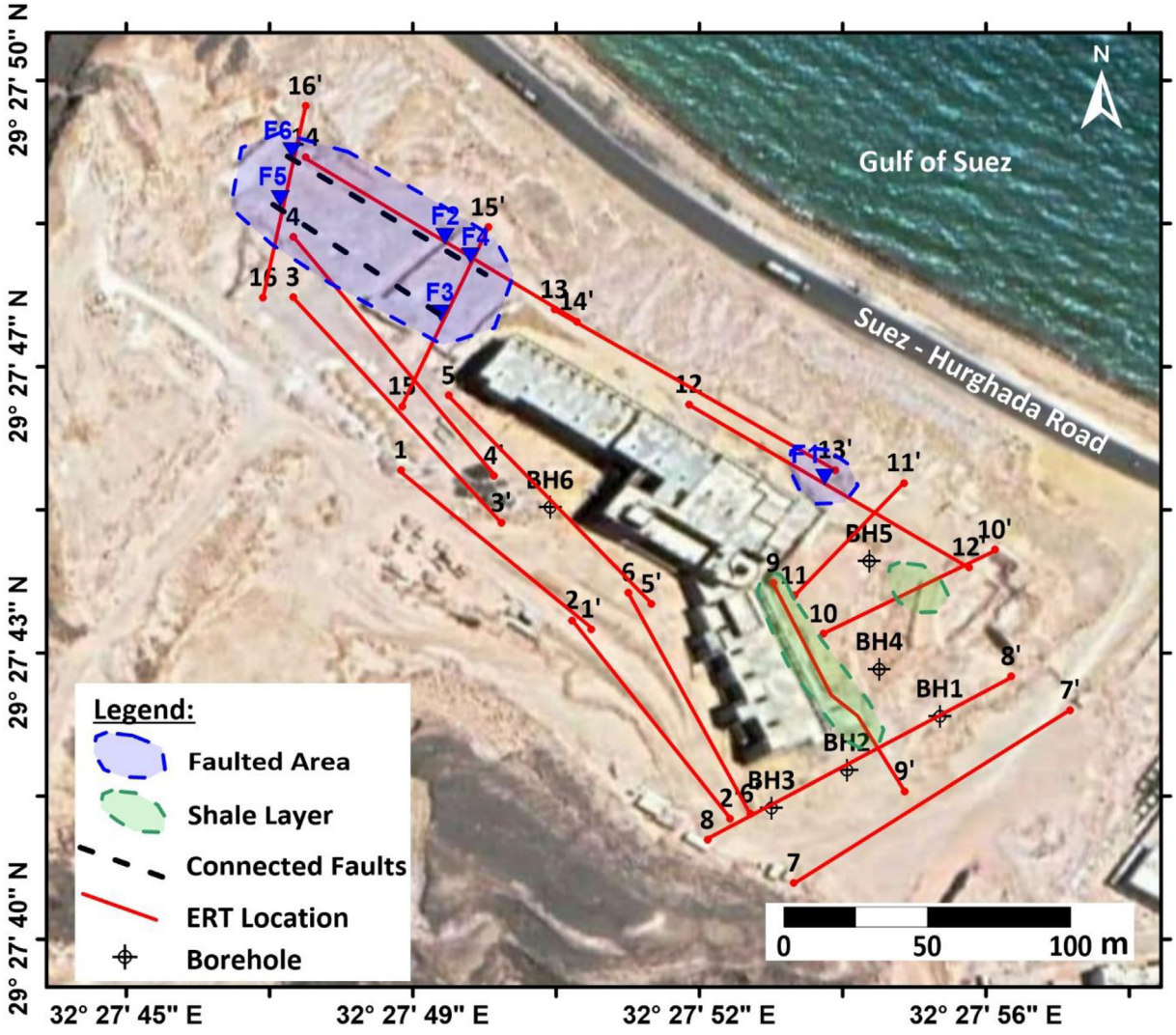


*Fig. 8. Google earth image showing the areas affected by faults and the location of the subsurface shale layer.*

number of faults (Fig. 8, faulted area labeled by blue polygon at ERT Profiles No. 14, 15, and 16).

## Funding

No funding was received for conducting this study.

### Conflicts of interest

The author reports there are no competing interests to declare.

## Acknowledgments

The author would like to thank the management of CAVO Resort Ain Sokhna for the hospitality during the fieldwork and to thank the editor and anonymous reviewers for their constructive comments and suggestions, which significantly improved the quality of this research.

## References

[1] Griffiths DH, Barker RD. Two-dimensional resistivity imaging and modeling in areas of complex geology. J Appl Geophys 1993;29:211–26.
[2] Dahlin T. The development of DC resistivity imaging techniques. Comput Geosci 2001;27:1019–29.
[3] Klitzsch E, List F, Pohlmann G, Handley R, Hermina M, Meissner B. Geological map of Egypt, conoco coral and Egyptian general petroleum company, Cairo, Egypt. 1987; NH 36 SW Beni Suef. Scale. 1:500,000.
[4] Abdallah AM, El Adin D. Stratigraphy of upper paleozoic rocks western side of the Gulf of Suez. Geol Surf Egypt 1965; 25:18. Paper No.
[5] Abdallah AM, El Adin D, Fahmy N. Stratigraphy of the lower mesozoic rocks, western side of the Gulf of Suez, Egypt. Cairo (Egypt), vol. 27. Egypt Geological Survey and Mineral Research Department; 1965. pp. 1–23. Paper No. 27.
[6] Abdelazeem M, Fathy MS, Khalifa MM. Integrating magnetic and stratigraphic data to delineate the subsurface features in and around new Galala City, Northern Galala Plateau, Egypt. NRIAG J Astron Geophys 2019;8:131–43.
[7] Said R. The geology of Egypt. Amsterdam: Elsevier Publishing Co; 1962. p. 396.
[8] Garfunkle Z, Bartov Y. The tectonics of the Suez rift. Geol Surv Isr Bull 1977;71:1–44.
[9] Chenet P, Colleta B, Letouzey J, Desforges G, Quset E, Zaghloul E. Structures associated with extensional tectonics in the Suez Rift, vol. 28. London: Geological Society; 1985. p. 551–8. Special Publications.
[10] Tapponnier P, Armijo R. Seismotectonics of northern Egypt. Terra Cogn 1985;5:171.
[11] Abdallah M. Structural geology of the area between El Galala El-Bahagia and Gabal Okheider, Egypt. Ph. D. Thesis, fac. Cairo, Egypt: . Sci, Ain Shams University; 1993. p. 199.
[12] Youssef M, Abdallah A. Structural geology of the southern part of the Cairo-Suez district, Egypt. Cairo: 5th Inter. Conf. for the Geology of the Middle East; 2003 (Abstract).
[13] Arnous MO, Aboulela HA, Green DR. Geo-environmental hazards assessment of the northwestern Gulf of Suez, Egypt. J Coast Conserv 2011;15:37–50.
[14] Cardarelli E, Cercato M, Di Filippo G. Assessing foundation stability and soil-structure interaction through integrated geophysical techniques: a case history in Rome (Italy). Near Surf Geophys 2007;5:141–7.
[15] Soupios PM, Georgakopoulos P, Papadopoulos N, Saltas V, Andreadakis A, Vallianatos F, et al. Use of engineering geophysics to investigate a site for a building foundation. J Geophys Eng 2007;4:94–103.
[16] Giocoli A, Magrì C, Vannoli P, Piscitelli S, Rizzo E, Siniscalchi A, et al. Electrical resistivity tomography investigations in the ufita Valley (southern Italy). Ann Geophys 2008;51:213–23.
[17] Sudha K, Israil M, Mittal S, Rai J. Soil characterization using electrical resistivity tomography and geotechnical investigations. J Appl Geophys 2009;67:74–9.
[18] Ayolabi EA, Folorunso AF, Oloruntola MO. Constraining causes of structural failure using electrical resistivity tomography (ERT): a case study of Lagos, Southwestern, Nigeria. Symp Appl Geophys Eng Environ Probl 2010;67: 877–93. https://doi.org/10.4133/1.3445528.
[19] Ayolabi EA, Folorunso AF, Jegede OE. An application of 2D electrical resistivity tomography in geotechnical investigations of foundation defects: a case study. J Geol Min Res 2012;4:142–51.
[20] Cercato M, De Donno G. Focusing on soil-foundation heterogeneity through high-resolution electrical and seismic tomography. Near Surf Geophys 2018;16:67–78.
[21] Butchibabu B, Khan PK, Jha PC. Foundation evaluation of a repeater installation building using electrical resistivity tomography and seismic refraction tomography. J Environ Eng Geophys 2019;24:27–38.
[22] Butchibabu B, Khan PK, Jha PC. Foundation evaluation of underground metro rail station using geophysical and geotechnical investigations. Eng Geol 2019;248:140–54.
[23] Cheng Q, Tao M, Chen X, Binley A. Evaluation of electrical resistivity tomography (ERT) for mapping the soil–rock interface in karstic environments. Environ Earth Sci 2019; 78:1–14.
[24] Diallo MC, Cheng LZ, Rosa E, Gunther C, Chouteau M. Integrated GPR and ERT data interpretation for bedrock identification at Cléricy, Québec, Canada. Eng Geol 2019;248: 230–41.
[25] Abudeif AM, Mohammed MA, Fat-Helbary RE, El-Khashab HM, Masoud MM. Integration of 2D geoelectrical resistivity imaging and boreholes as rapid tools for the geotechnical characterization of construction sites: a case study of New Akhmim city, Sohag, Egypt. J Afr Earth Sci 2020;163:103734.
[26] Dhamiry NM, Zouaghi T. Near-surface geophysical surveys for bedrock investigation and modeling for grain silos site, Yanbu City, Western Saudi Arabia. Model Earth Syst Environ 2020;6:51–61.
[27] Loke MH. Electrical imaging surveys for environmental and engineering studies. Cang Mind Lorong 1999; 6574525:57.
[28] Geomative Company. GD-10 2D/3D resistivity imaging system, GD-10 Supreme user's manual. ST Geomative Co., Ltd.; 2019.